Thomas von Arx[1]
Scott Lozanoff[2]
Michael M. Bornstein[3,4]

[1] Department of Oral Surgery and Stomatology, School of Dental Medicine, University of Bern, Switzerland
[2] Department of Anatomy, Biochemistry and Physiology, John A. Burns School of Medicine, University of Hawaii, Honolulu, USA
[3] Oral and Maxillofacial Radiology, Applied Oral Sciences and Community Dental Care, Faculty of Dentistry, The University of Hong Kong, Prince Philip Dental Hospital, Hong Kong SAR, China
[4] Department of Oral Health & Medicine, University Center for Dental Medicine Basel UZB, University of Basel, Basel, Switzerland

CORRESPONDENCE
Prof. Dr. Thomas von Arx
Klinik für Oralchirurgie und Stomatologie
Zahnmedizinische Kliniken der Universität Bern
Freiburgstrasse 7
CH-3010 Bern
Tel. +41 31 632 25 66
Fax +41 31 632 25 03
E-mail:
thomas.vonarx@zmk.unibe.ch

SWISS DENTAL JOURNAL SSO 130: 768–784 (2020)
Accepted for publication:
26 March 2020

Extraoral anatomy in CBCT – a literature review

Part 4: Pharyngocervical region

KEYWORDS
Anatomy
CBCT
Pharynx
Cervical spine
Hyoid bone
Styloid process

SUMMARY
This review about extraoral anatomy depicted in cone beam computed tomography describes the pharyngocervical region. Large (≥ 8 × 8 cm) field of views of the maxilla and/or mandible will inevitably depict the pharyngocervical region that comprises the posterior upper airway, the pharyngeal part of the digestive tract, as well as the cervical segment of the spine. The latter consists of seven cervical vertebrae (C1–C7) with corresponding distinctive features, i.e., the atlas (C1) and the axis (C2). In addition, cervical vertebrae serve as references for the vertical position of anatomical structures. For instance, C4 is a typical landmark since it generally denotes the level of the chin, of the body of the hyoid bone, of the base of the epiglottis, and of the bifurcation of the common carotid artery, respectively. The pharynx, which is functionally involved in respiration, deglutition, and vocalization, extends from the lower aspect of the skull base to the esophagus. Anatomically, the pharynx is divided into three segments, i.e. the nasopharynx, the oropharynx, and the laryngopharynx. All communicate anteriorly with corresponding cavities, i.e. the nasal cavities, the oral cavity, and the larynx. Although not directly located within the pharyngocervical region, the hyoid bone and the styloid process are also discussed in this review, since both structures are commonly visible on CBCT images of this region.

Introduction

This last of four literature reviews about extraoral anatomy in cone beam computed tomography (CBCT) refers to the pharyngocervical region. This region contains the posterior upper airway, the pharynx, and the cervical segment of the spine. When taking a CBCT scan of the posterior maxilla and/or mandible, the pharynx or even the cervical spine become partly or fully visible on the imaged radiographic volume (White et al. 2015). However, the extent of the anatomical presentation is dependent on the chosen field of view (FOV).

The pharynx, being part of the digestive as well as the respiratory system, is embedded in the complex spatial anatomy of the neck and, due to its function and location, represents a very intricate region (Lomoschitz et al. 2000). While the structures of the pharynx mainly include soft tissues (mucosal layers, muscles, vessels, nerves), those of the cervical region also include bony features, such as the hyoid bone and the cervical vertebrae.

Pharynx

The pharynx extends from the lower aspect of the skull base to the opening of the esophagus, i.e., the pharyngo-esophageal sphincter that is located at the level of the sixth cervical vertebra (C6) (Fig. 1–7). It connects the nasal and oral cavities with the trachea and the esophagus, respectively. Functionally, the pharynx is involved in respiration, deglutition, and vocalization. The anatomy of the upper airway helps to accommodate these functions (Lun et al. 2016). The pharynx has a half-cylindrical shape and is approximately 13 cm long (Nemec et al. 2009). The maximum width of the pharynx is found in the laryngopharynx with mean distances in CT of 4.1 ± 0.4 cm (males) and 3.6 ± 0.4 cm (females) (Inamoto et al. 2015).

From an anatomical perspective, the pharynx is located behind the choanae, the tongue, and the larynx. Consequently, the pharynx is divided into three segments, i.e., the nasopharynx, the oropharynx, and the laryngopharynx (https://sketchfab.com/3d-models/midsagittal-view-of-the-pharynx-6251df477323492d99b0a03e9750822e). Each of these segments has an anterior opening. From a structural perspective, the pharynx is a musculofascial tube encompassing the three pharyngeal constrictor muscles (superior, middle, and inferior) and their respective fasciae. The prevertebral fascia overlying the *longus colli* and *longus capitus* muscles also contributes to the posterior pharyngeal wall (Becker & Hwang 2013).

Lun et al. (2016) investigated the upper airway anatomy with ultrasound in healthy volunteers at three levels (velo-, oro-, and hypopharyngeal levels). They demonstrated that during deep inspiration, the anteroposterior dimensions of the three airway levels presented larger values than after expiration ($p < 0.001$). In contrast, lateral diameters of the pharynx at these three anatomic levels were greater at the end of deep expiration than those at the end of deep inspiration ($p < 0.001$).

Nasopharynx (epipharynx, rhinopharynx, pars nasalis pharyngis)

The nasopharynx is the uppermost portion of the pharynx. Anteriorly, it communicates via the choanae with the bilateral nasal cavities. Superiorly, the nasopharynx extends to the skull base (sphenoid and occipital bones). Posteriorly, it is bordered by the superoposterior wall of the pharynx. Inferiorly, the nasopharynx extends to the soft palate and the uvula. Some authors differentiate a so-called velopharynx extending caudally from the level of the hard palate to the tip of the uvula (White et al. 2015), and as such representing the lower portion of the nasopharynx. In a CT study of 25 healthy Japanese subjects, the average length of the soft palate (distance from the posterior nasal spine to the tip of the uvula) was 38.6 ± 6.6 mm and the height of the velopharynx was 32.1 ± 7.5 mm (Shigeta et al. 2010). Males had significantly greater soft palate length ($p = 0.002$) and velopharynx height ($p = 0.006$) compared to females.

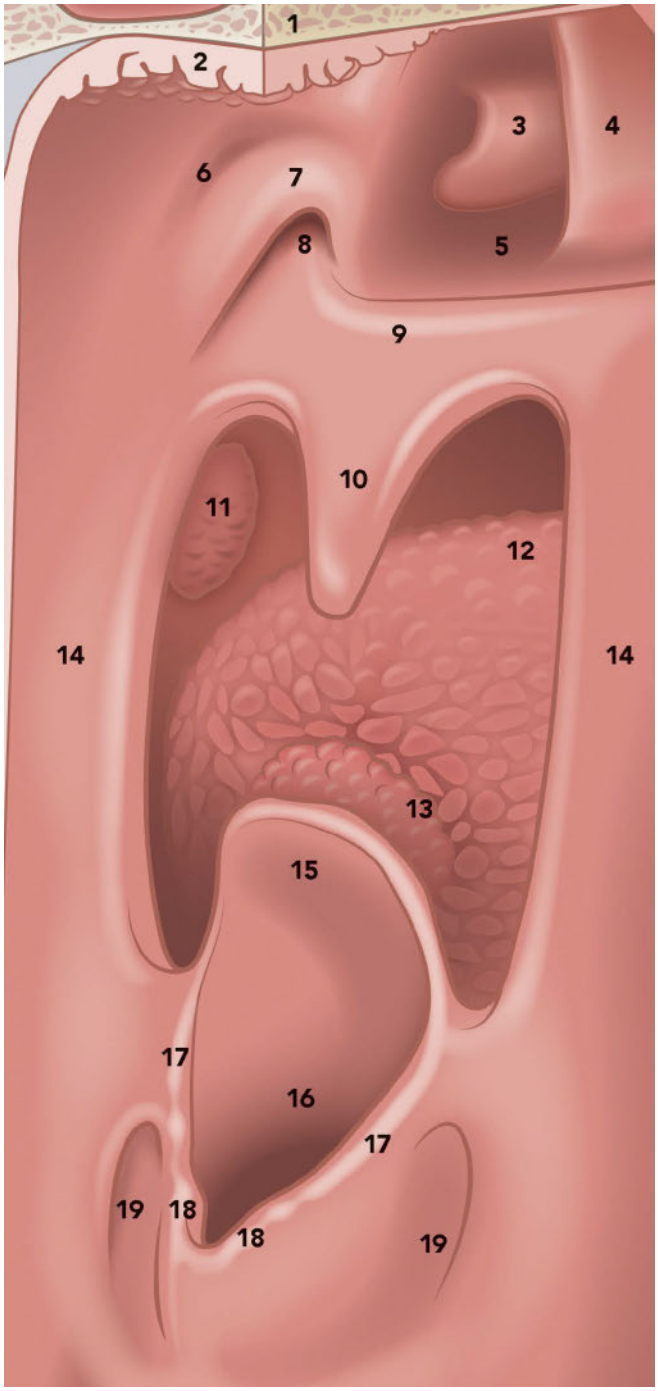

Fig. 1 Schematic illustration of the pharynx (posterior view).
1 = occipital bone; 2 = roof of nasopharynx with adenoids (pharyngeal tonsils); 3 = left inferior nasal concha; 4 = nasal septum (vomer); 5 = left choana; 6 = left pharyngeal recess (fossa of Rosenmuller); 7 = torus of left pharyngotympanic tube; 8 = opening of left pharyngotympanic tube; 9 = soft palate; 10 = uvula; 11 = left palatal tonsil; 12 = dorsum of tongue; 13 = base of tongue; 14 = lateral pharyngeal wall; 15 = epiglottis; 16 = laryngeal inlet; 17 = aryepiglottic fold; 18 = corniculate tubercle; 19 = piriform recess.

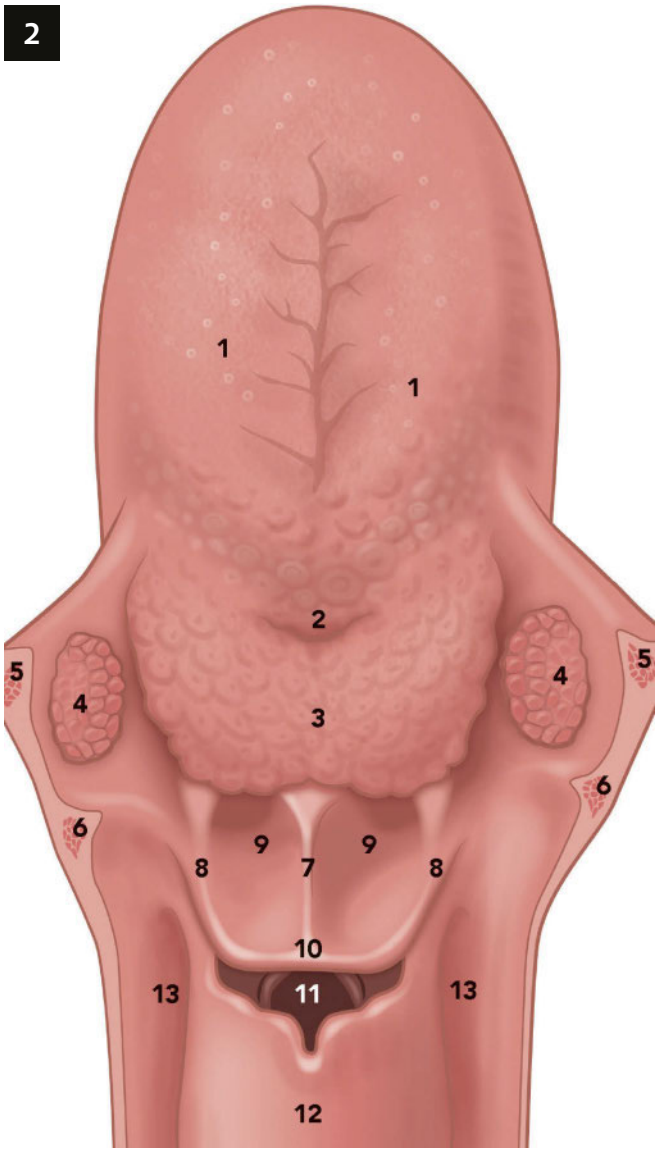

Fig. 2 Schematic illustration of the orolaryngopharynx (superior view). 1 = dorsum of tongue; 2 = sulcus terminalis; 3 = base of tongue; 4 = palatal tonsil; 5 = palatoglossus muscle; 6 = palatopharyngeus muscle; 7 = plica glossoepiglottica mediana; 8 = plica glossoepiglottica lateralis; 9 = vallecula epiglottica; 10 = superior border of epiglottis; 11 = laryngeal inlet; 12 = posterior wall of larynx; 13 = piriform recess.

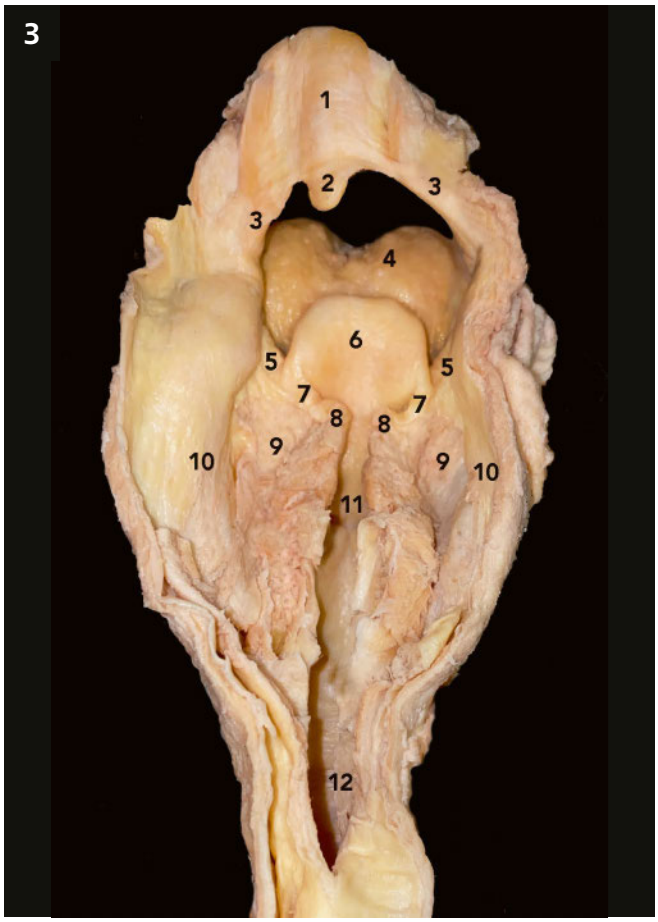

Fig. 3 Cadaveric specimen showing the orolaryngopharynx (posterior view). 1 = soft palate; 2 = uvula; 3 = palatoglossus muscle; 4 = dorsum of tongue; 5 = plica glossoepiglottica lateralis; 6 = epiglottis; 7 = aryepiglottic fold; 8 = corniculate tubercle; 9 = piriform recess; 10 = lateral pharyngeal wall; 11 = laryngeal inlet; 12 = trachea.

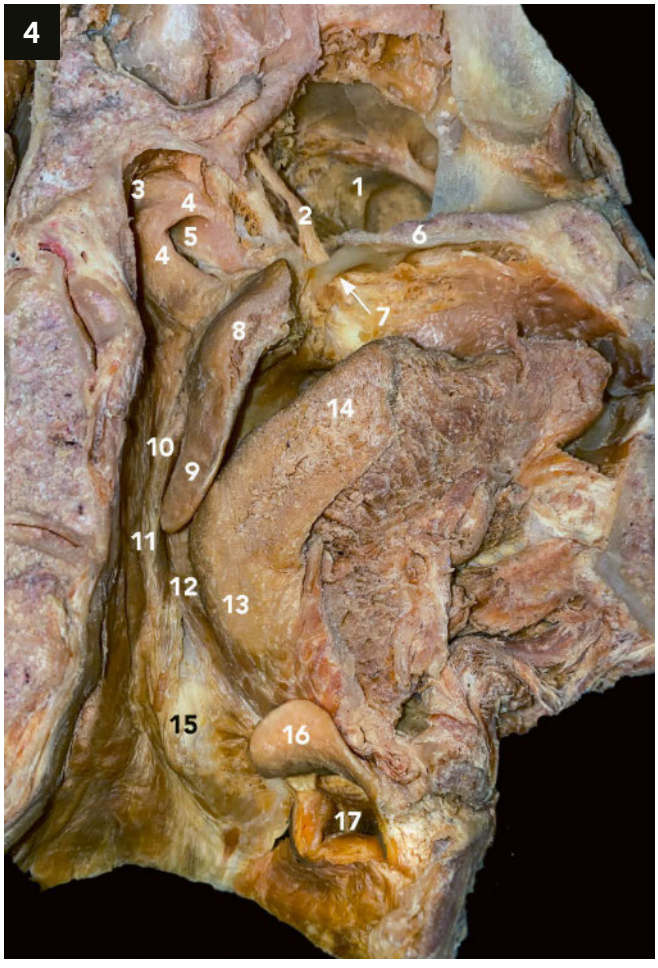

Fig. 4 Cadaveric view of the pharynx and contiguous structures (lateral view). 1 = left maxillary sinus; 2 = greater palatine nerve; 3 = left pharyngeal recess (fossa of Rosenmuller); 4 = torus of left pharyngotympanic tube; 5 = opening of left pharyngotympanic tube; 6 = hard palate; 7 = greater palatine foramen; 8 = soft palate; 9 = uvula; 10 = salpingopharyngeal muscle; 11 = palatopharyngeus muscle; 12 = palatoglossus muscle; 13 = base of tongue; 14 = dorsum of tongue; 15 = hyoid bone; 16 = epiglottis; 17 = laryngeal inlet.

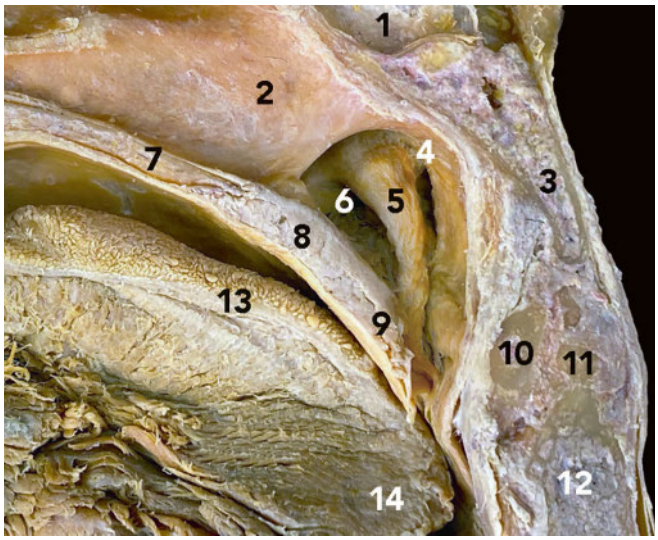

Fig. 5 Midsagittal cadaveric dissection with medial view of the right nasopharynx.
1 = sphenoid sinus; 2 = vomer; 3 = clivus; 4 = right pharyngeal recess (fossa of Rosenmuller); 5 = torus of right pharyngotympanic tube; 6 = opening of right pharyngotympanic tube; 7 = hard palate; 8 = soft palate; 9 = uvula; 10 = anterior arch of C1 (atlas); 11 = odontoid process of C2 (axis); 12 = body of C2; 13 = dorsum of tongue; 14 = base of tongue.

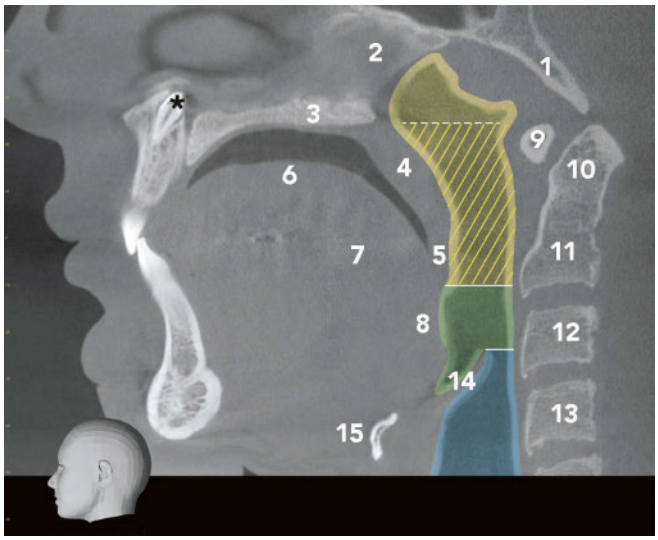

Fig. 6 Midsagittal CBCT image of a 21-year-old male highlighting the nasopharynx (yellow), the oropharynx (green), and the laryngopharynx (blue). The hatched area represents the so-called velopharynx. Inverted mesiodens as incidental finding (*).
1 = clivus (occipital bone); 2 = vomer; 3 = hard palate; 4 = soft palate; 5 = uvula; 6 = dorsum of tongue; 7 = body of tongue; 8 = base of tongue; 9 = anterior arch of C1 (atlas); 10 = odontoid process of C2 (axis); 11 = body of C2; 12 = body of C3; 13 = body of C4; 14 = epiglottis; 15 = hyoid bone (median body).

The velopharynx is a complex anatomical structure made up of five paired muscles *(levator veli palatini, tensor veli palatini, palatoglossus, palatopharyngeus,* and *superior pharyngeal constrictor)* and one single muscle *(musculus uvulae)*. It is responsible for separation of the oral and nasal cavities during speech and swallowing. Incompetence of this mechanism can lead to hypernasality, snoring and/or nasopharyngeal regurgitation (Raol & Hartnick 2015). The velopharynx is also considered the most collapsible part of the pharynx (Shigeta et al. 2010).

The adenoids (pharyngeal tonsils) are lymphatic tissue located on the superoposterior wall of the nasopharynx. The opening of the pharyngotympanic tube (connecting to the middle ear) is found in the lateral wall of the nasopharynx. This *ostium tubae* is usually located 1–1.5 cm posterior to the dorsal end of the inferior nasal turbinate (Nemec et al. 2009). A semicircular elevation superoposterior to this orifice corresponds with the most medial part of the cartilaginous pharyngotympanic tube (also known as salpinx, trumpet, or Eustachian tube). The deep recess of the nasopharynx located posterior to the Eustachian ostium is known as the pharyngeal recess or fossa of Rosenmuller (Nemec et al. 2009; Becker & Hwang 2013) while the rim of cartilage protruding into the nasopharynx is termed the *torus tubarius*.

Fig. 7 Midsagittal CBCT image of a 68-year-old female (purple lines represent the different levels of axial CBCT images shown in cropped Fig. 7A–7H):
- through roof of nasopharynx (Fig. 7A)
- at the level of the openings of the pharyngotympanic tubes (Fig. 7B)
- at the level of the hard palate (Fig. 7C)
- at the midlevel of the soft palate (Fig. 7D)
- at the level of the body of C2 (Fig. 7E)
- at the level of the tip of the epiglottis and C3 (Fig. 7F)
- at the level of the hyoid bone (Fig. 7G)
- at the level of the inferior portion of C4 (Fig. 7H)

1 = clivus (occipital bone); 2 = vomer; 3 = hard palate; 4 = soft palate; 5 = dorsum of tongue; 6 = body of tongue; 7 = base of tongue; 8 = anterior arch of C1 (atlas); 9 = odontoid process of C2 (axis); 10 = body of C2; 11 = body of C3; 12 = body of C4; 13 = epiglottis; 14 = hyoid bone (median body)

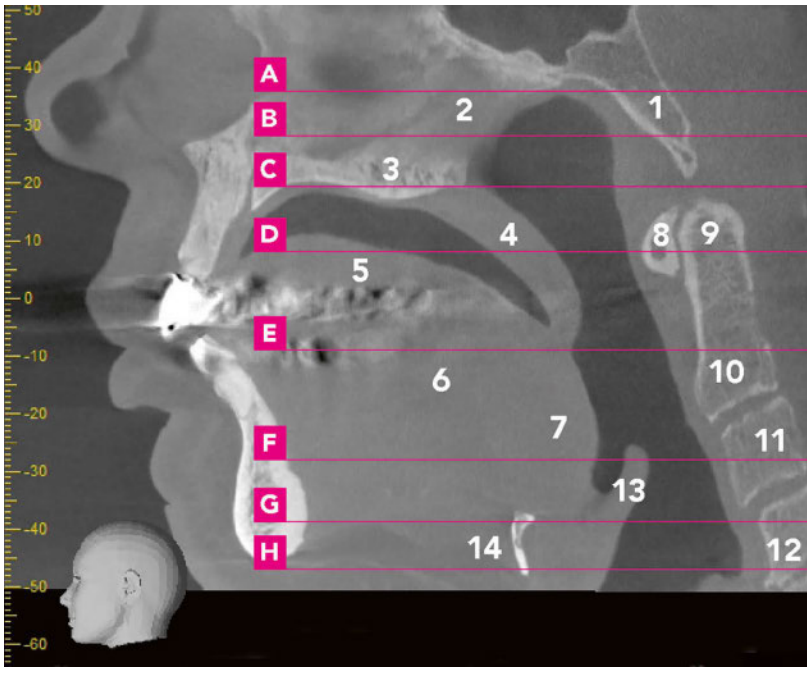

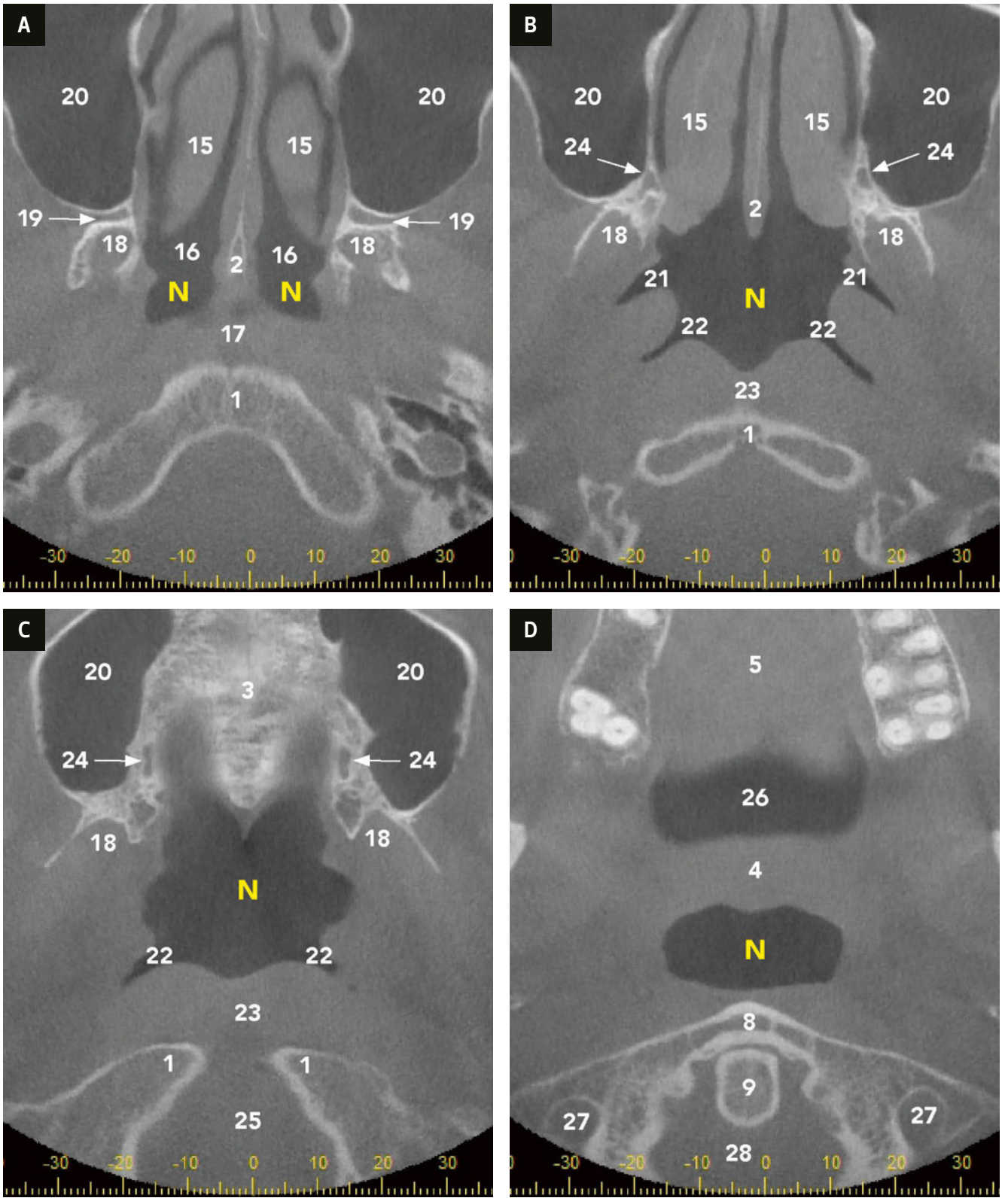

Fig. 7A–H Axial CBCT images of a 68-year-old female:
- through roof of nasopharynx (Fig. 7A)
- at the level of the openings of the pharyngotympanic tubes (Fig. 7B)
- at the level of the hard palate (Fig. 7C)
- at the midlevel of the soft palate (Fig. 7D)
- at the level of the body of C2 (Fig. 7E)
- at the level of the tip of the epiglottis and C3 (Fig. 7F)
- at the level of the hyoid bone (Fig. 7G)
- at the level of the inferior portion of C4 (Fig. 7H)

1 = clivus (occipital bone); 2 = vomer; 3 = hard palate; 4 = soft palate; 5 = dorsum of tongue; 6 = body of tongue; 7 = base of tongue; 8 = anterior arch of C1 (atlas); 9 = odontoid process of C2 (axis); 10 = body of C2; 11 = body of C3; 12 = body of C4; 13 = epiglottis; 14 = hyoid bone (median body); 15 = inferior concha; 16 = choana; 17 = roof of nasopharynx (mucosa); 18 = pterygoid fossa; 19 = pterygopalatine fossa; 20 = maxillary sinus; 21 = opening of pharyngotympanic tube; 22 = pharyngeal recess (fossa of Rosenmuller); 23 = retropharyngeal wall; 24 = greater palatine canal; 25 = foramen magnum; 26 = oral cavity; 27 = transverse foramen; 28 = vertebral foramen;

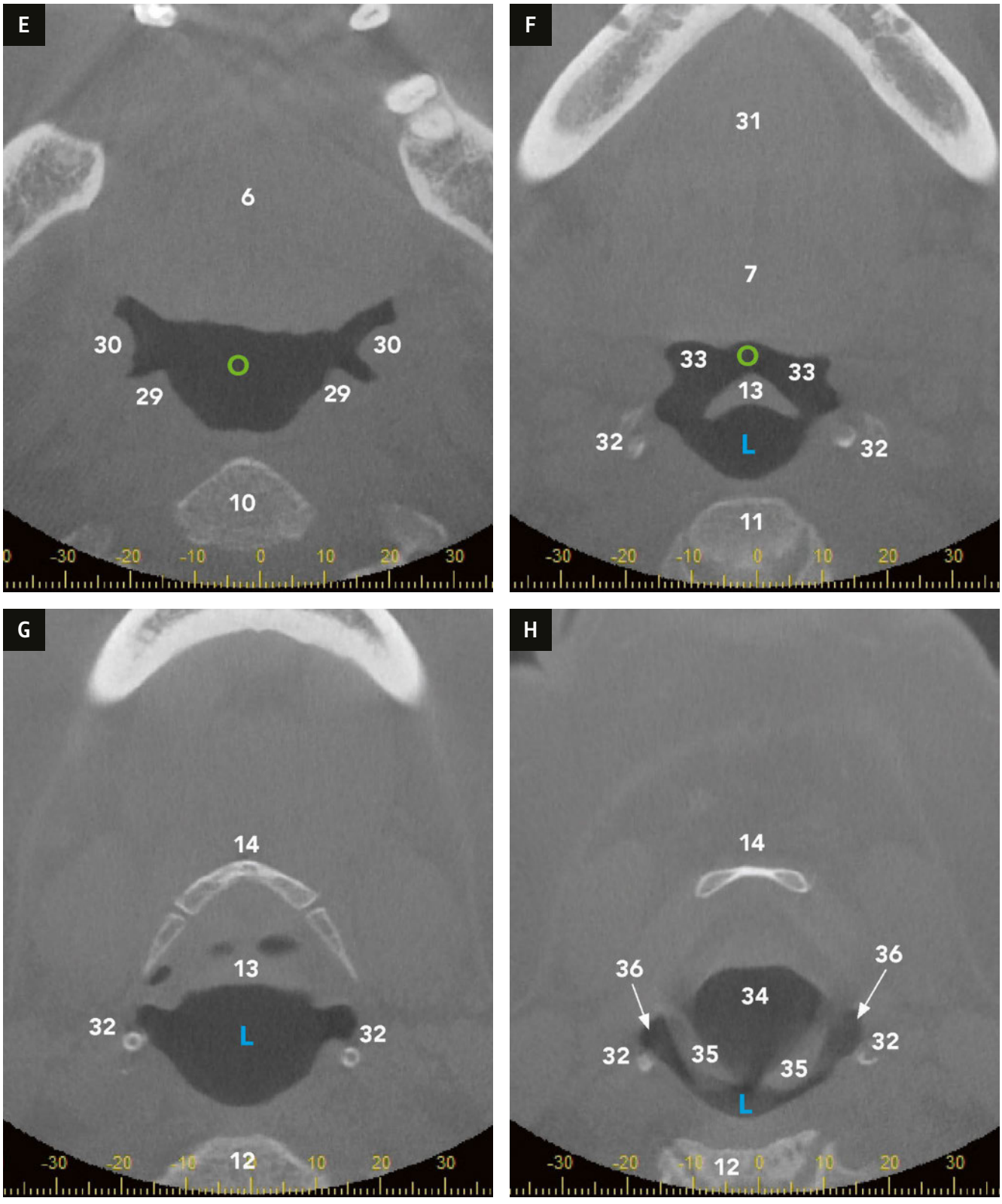

29 = palatopharyngeal pillar; 30 = palatal tonsil; 31 = floor of mouth; 32 = greater horn (cornu major) of hyoid bone; 33 = vallecula epiglottica; 34 = laryngeal inlet; 35 = aryepiglottic fold; 36 = piriform recess; N = naso-pharynx; O = oropharynx; L = laryngopharynx.

The salpingopharyngeal fold extends inferolaterally from the tube and blends into the lateral wall of the nasopharynx. It contains the salpingopharyngeal muscle, a small portion of the palatopharyngeus muscle.

In approximately 20% of the population, a bulge along the posterior pharyngeal wall due to contraction of the superior pharyngeal constrictor may be seen. First described in 1863 by Passavant and therefore termed Passavant's ridge, it is believed by some to aid in velopharyngeal closure, although this remains controversial (Raol & Hartnick 2015).

Oropharynx (mesopharynx, pars oralis pharyngis)

When a patient is asked to open wide this mouth, the oropharynx can be seen in the far depth. The oropharynx extends from the soft palate/uvula down to the epiglottis (medially) and the aryepiglottic folds (laterally). Hence, it is located posterior to the oral cavity and the tongue. The communication between the oral cavity and the oropharynx is also known as the *isthmus faucium*. In clinical oncology, the oropharynx is generally divided into four distinct components: (i) the base of the tongue; (ii) the soft palate; (iii) the palatine tonsillar fossae; and (iv) the pharyngeal walls (Fossum et al. 2017).

With regard to the cervical spine, the oropharynx is roughly located at the level of the axis down to the interspace of the second and third vertebrae (C2/C3). The oropharynx also encompasses the lateral and posterior oropharyngeal walls that are formed by the superior and middle pharyngeal constrictors (Nemec et al. 2009). The lateral pharyngeal walls contain the anterior and posterior tonsillar pillars that are formed by the palatoglossus and palatopharyngeus muscles, respectively. Palatine tonsils are located in the tonsillar fossae bounded by these pillars (Gun & Ozer 2015).

The anterior wall of the oropharynx is formed by the base of the tongue that projects posteriorly. The base of the tongue – also known as pharyngeal part of tongue – begins behind the *sulcus terminalis* circumvallate papillae. Lingual tonsils (lymphoid tissue), which are contiguous with the palatine tonsils, are found on the lateral aspects of the tongue base (Gun & Ozer 2015).

Inamoto et al. (2015) assessed the volume of the oropharynx in 54 healthy subjects using multidetector CT. The volume amounted to 19.2 ± 4.9 cm^3 in males and to 13.5 ± 4.3 cm^3 in females. The difference was statistically significant. In a CBCT study of the oropharynx of 10 healthy subjects, Ogawa et al. (2007) reported minimum anteroposterior and lateral dimensions of 7.8 ± 3.3 mm and 16.2 ± 6.8 mm, respectively. The area at the smallest cross section of the oropharynx amounted to 147 ± 112 mm^2.

The upper (lingual) surface of the epiglottis as well as the glossoepiglottic folds, one median *(plica glossoepiglottica mediana)* and two lateral folds *(plicae glossoepiglotticae laterales)* sweeping to the posterior base of the tongue, are commonly considered parts of the oropharynx. These three glossoepiglottic folds line two mucosal pouches, also known as the *valleculae epiglotticae*. The *valleculae* are characterized as depressions between the posterior root of the tongue and the upper surface of the epiglottis.

The oropharynx contains a circular area of mucosal-associated lymphoid tissue (MALT) known as Waldeyer's tonsillar ring. Included in Waldeyer's ring are the palatine and lingual tonsils of the oropharynx, but also the pharyngeal and tubal tonsils of the nasopharynx. Waldeyer's ring is considered to be the guardian of the oropharynx (Fossum et al. 2017).

Laryngopharynx (hypopharynx, pars laryngea pharyngis)

The laryngopharynx is the most inferior section of the pharynx and lies behind the larynx. It communicates anteriorly with the laryngeal inlet. The posterior wall of the laryngopharynx is formed by the inferior pharyngeal constrictor muscle. This muscle comprises two subcomponents including thyropharyngeal and cricopharyngeal portions. The cricopharyngeal portion combines with fibers from the upper esophagus to form a sphincter that prevents air from entering the esophagus prior to receiving the food bolus. This pharyngeal mucosa between the thyropharyngeal and cricopharyngeal portions of the inferior constrictor muscle (Killian's dehiscence) can herniate forming a hypopharyngeal diverticulum (Zenker's diverticulum) potentially causing dysphagia, frequent regurgitation and aspiration pneumonia.

The laryngopharynx extends from the floor of the *valleculae* (level C3/C4) to the portion of the pharynx funneling into the esophagus, located roughly at the lower border of the cricoid cartilage (level C5/C6) (Nemec et al. 2009). Hence, the epiglottis, a fibroelastic cartilage, is the natural border between the oro- and the laryngopharynx. Upon deglutition, the epiglottis closes the opening of the larynx to prevent the food bolus from entering the trachea.

Between the lateral glossoepiglottic fold (also known as the pharyngoepiglottic fold) and the lateral pharyngeal wall, a vertical depression (piriform recess or sinus) extends caudally on either side of the laryngopharynx. The piriform sinuses (shape of an inverted pear) end inferiorly at the *cricopharyngeus* muscle that is the most inferior structure of the pharynx and serves as the valve at the top of the esophagus. The average height of the pyriform sinus assessed with CT was 20.1 ± 4.4 mm in males and 16.6 ± 4.0 mm in females (Inamoto et al. 2015).

Cervical spine

The cervical spine consists of seven vertebrae (C1 to C7) (Fig. 8–11). The two uppermost cervical vertebrae (atlas and axis) present a special morphology while the lower five cervical vertebrae show similar characteristics to the thoracic vertebrae. The cervical vertebrae, as a group, produce a lordotic curve, and they have the greatest intervertebral disc height, hereby increasing the range of motion (Waxenbaum & Futterman 2019). As a whole, the cervical spine is responsible for supporting the weight of the cranium and allowing motion of the head and neck (Kaiser & Lugo-Pico 2019). From a functional perspective, the cervical spine has been divided into three zones: the suboccipital zone centered on the C1 vertebra; a transitional zone formed by the C2 vertebra; and the typical zone, encompassing the C3–C7 vertebrae (Bogduk & Mercer 2000). The cervical skeleton is also a bony framework for the vertebral arteries in their course from the aortic arch to the cranial fossa (Wysocki et al. 2003).

Cervical vertebrae may be used as references for the vertical position of pharyngeal structures (Mirjalili et al. 2012). The authors evaluated 52 CT scans of the neck from supine adults with a standardized head position. The hard palate was consistently found at the vertebral level of C1 (anterior arch of atlas). The center of the body of the hyoid bone was most frequently located (54%) at C4. The superior limit of the *laminae* of the thyroid cartilage was mainly observed at C4 in woman (60%) but at C5 in men (52%) (Mirjalili et al. 2012).

Liu et al. (2017) assessed cervical landmarks both in flexion and extension lateral radiographs of the cervical spine. The

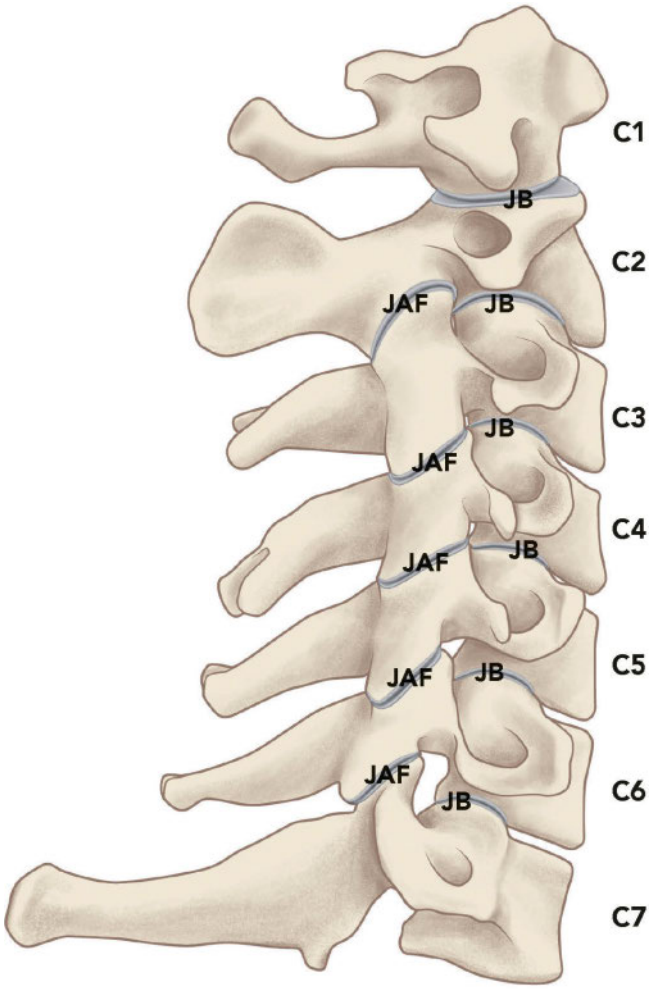

Fig. 8 Schematic illustration of the cervical spine (lateral view of right side). Note the prominent spinous process of C7.
JB = central joints between bodies of cervical vertebrae; JAF = bilateral joints between articulating facets of cervical vertebrae.

mandibular angle was the most consistent landmark with respect to the cervical spine and projected most frequently to level C2 (flexion and extension films), whereas the hyoid bone was at the interspace C3–C4 (flexion films) and C3 (extension films), respectively. Civalek et al. (2007) evaluated landmarks in 30 fresh cadavers. The bifurcation of the common carotid artery was mostly found at the level of C4 (78%). Also, the superior ganglion of the cervical sympathetic chain was located at the C4 vertebra. Drainage of the facial vein into the internal jugular vein was mostly seen at the level of C3–C4.

C1 (atlas)

Cervical vertebra C1, also known as atlas, is the uppermost part of the vertebral column and supports the head atlas (https://sketchfab.com/3d-models/c1-0f356f60803d41a690d475e0ca1240d0). The atlas connects to the skull via the atlanto-occipital joint. The latter includes the bilateral superior concave articulating facets of C1 and the convex condyles of the occipital bone. The atlas differs in structure from all other cervical vertebrae and is also the most variable vertebra in man (Wysocki et al. 2003). In contrast to the other vertebrae, the atlas has no body and no spinous process. It consists of an anterior and posterior arch and has a ring-like shape. The lateral bony masses have a transverse foramen for the vertebral artery and vein. According to Bogduk & Mercer (2000), the atlas resembles in structure the occipital bone, as can be seen in axial scans. In function, it more closely operates with the head rather than with the rest of the cervical spine.

C2 (axis)

Cervical vertebra C2, also known as axis (Latin *axis* = axle), is also unique compared to the other cervical vertebrae (https://sketchfab.com/3d-models/c2-a9238d092f5e4371828acb81fc3ff7fe). It has a prominent superior bony projection, the dens axis/epistropheus or odontoid process. The latter articulates with the inner facet surface of the anterior arch of the atlas (median atlantoaxial joint). This joint is the pivot upon which the atlas rotates (Bogduk & Mercer 2000), thus enabling side-to-side movements of the head. The axis has no transverse foramen in the lateral parts but displays posteriorly a bifid spinous process. Although a small degree of flexion and extension is possible between the axis and the atlas, the cardinal movement between these two vertebrae is axial rotation.

C3–C6

The vertebrae C3 to C6 exhibit the typical features of vertebrae in general, i.e., a strong anterior body, lateral masses with superior and inferior articular facets (that contribute to the zyga-

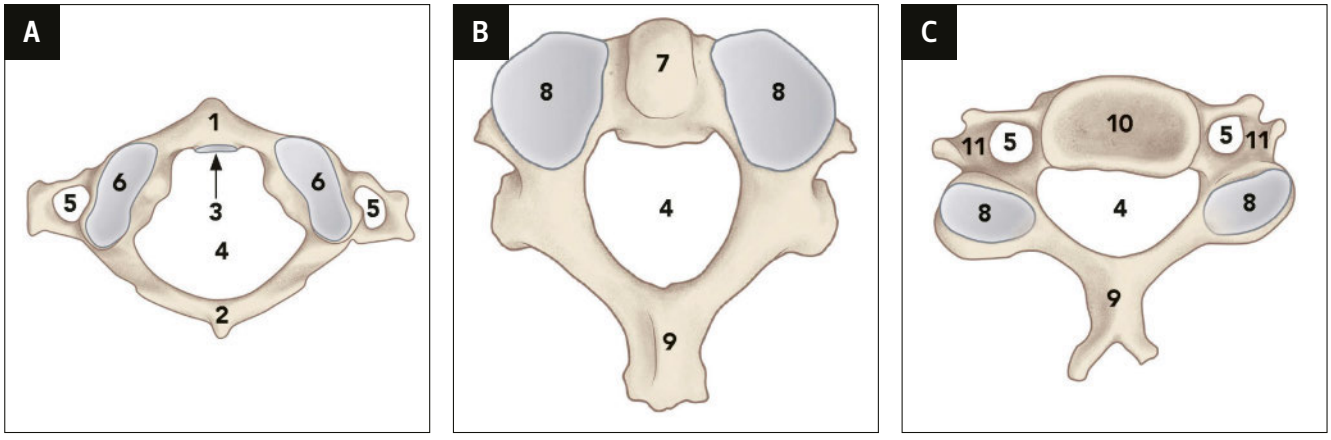

Fig. 9 Schematic illustrations (superior views) of atlas (A), axis (B) and typical C3–C6 vertebra (C).
1 = anterior arch; 2 = posterior arch; 3 = facet for dens of axis; 4 = vertebral foramen; 5 = transverse foramen, 6 = facet of atlanto-occipital joint; 7 = dens axis; 8 = superior articular facet; 9 = spinous process; 10 = body of vertebra; 11 = transverse process with anterior and posterior tubercles.

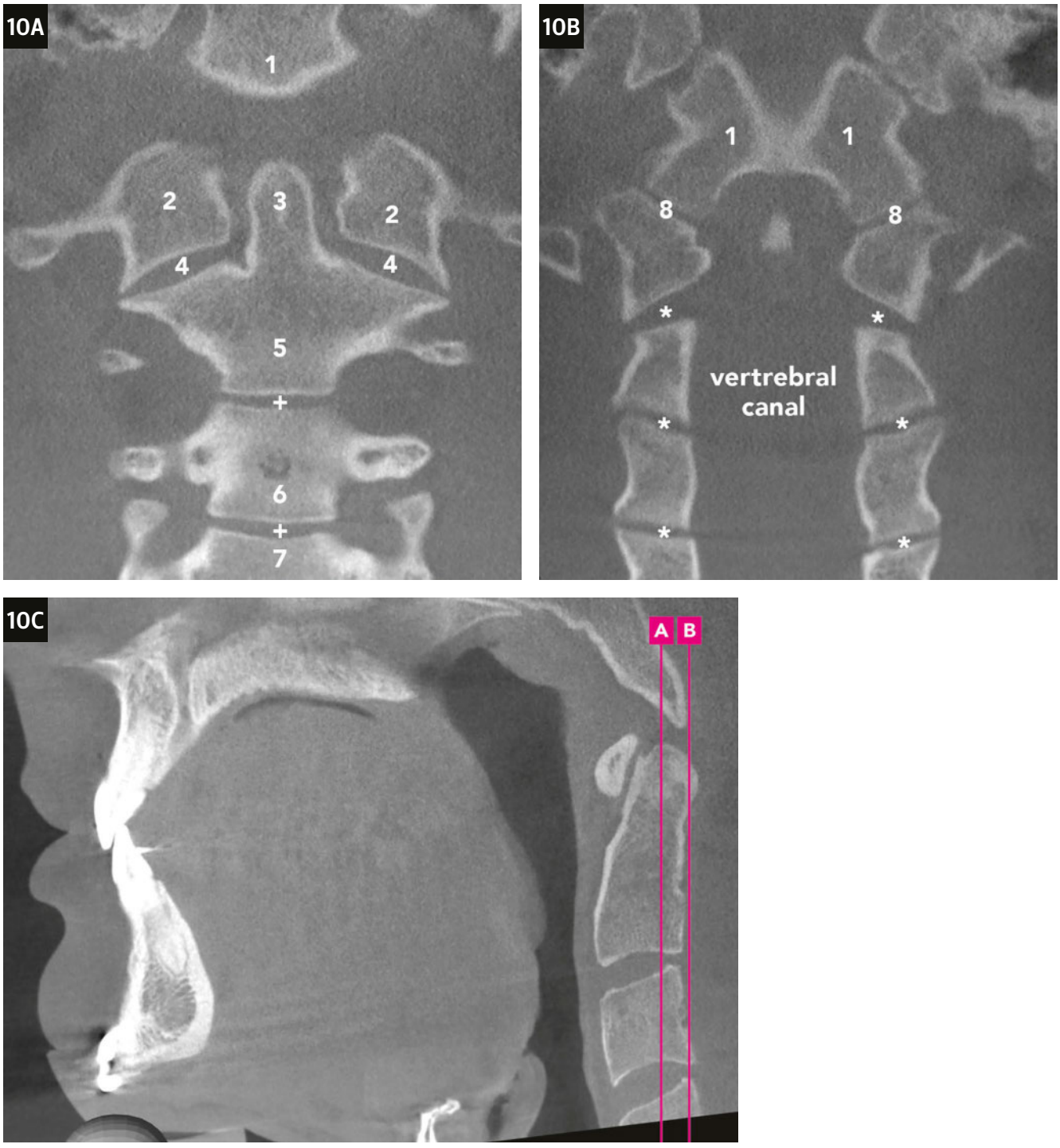

Fig. 10 CBCT sections through upper cervical vertebral columns in a 20-year-old male: (A) coronal section through bodies of vertebrae, (B) coronal section through vertebral canal. Fig. C shows the relative position of the coronal images relative to the midsagittal image.
1 = occipital bone; 2 = atlas; 3 = dens axis; 4 = facet articulations between atlas and axis; 5 = body of axis; 6 = body of C3; 7 = body of C4; 8 = atlanto-occipital joint; + = central joints between bodies of cervical vertebrae; * = bilateral joints between articulating facets of cervical vertebrae.

Fig. 11 Midsagittal CBCT image of a 13-year-old male (purple lines represent different levels of axial CBCT images shown in Fig. 11A–11D):
- at midlevel of nasopharynx (Fig. 11A)
- through body of C3 (Fig. 11B)
- through upper part of body of C4 (Fig. 11C)
- through lower part of body of C4 (Fig. 11D)

1 = hard palate; 2 = soft palate; 3 = anterior arch of atlas; 4 = odontoid process of C2 (axis); 5 = body of C2; 6 = dorsum of tongue; 7 = base of tongue; 8 = epiglottis; 9 = body of C3; 9a = posterior arch of C3; 9b = spinous process of C3; 10 = body of C4; 10a = spinous process of C4; 11 = hyoid bone (median body); 11a = greater horns; 12 = laryngeal inlet; 13 = ascending ramus of mandible; 14 = styloid process; 15 = vertebral foramen; 16 = occipital bone; 17 = prominence of chin; 18 = transverse foramen; 19 = inferior border of chin; 20 = aryepiglottic fold; 21 = piriform recess; * = atlanto-occipital joint; + = bilateral joints between articulating facets of cervical vertebrae; N = nasopharynx; L = laryngopharynx.

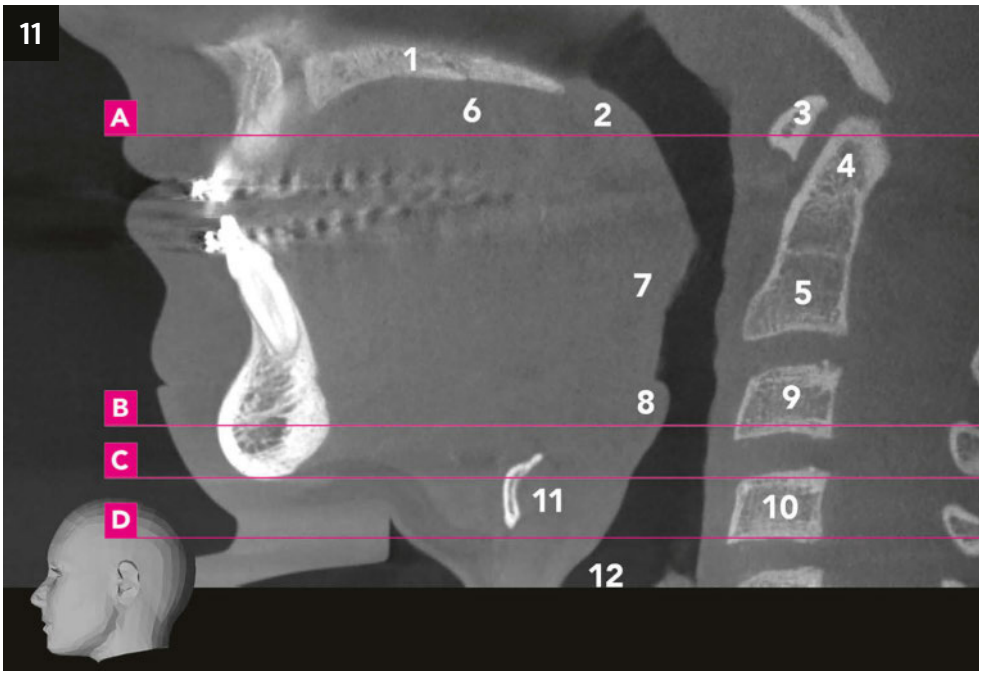
11
1
6
2
3
4
A
7
5
B
8
9
C
11
10
D
12

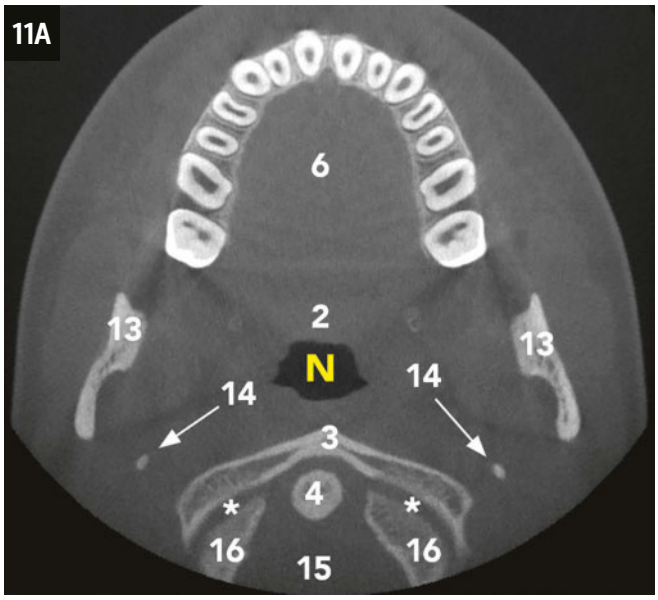
11A
6
13
2
N
13
14
14
3
4
*
*
16
15
16

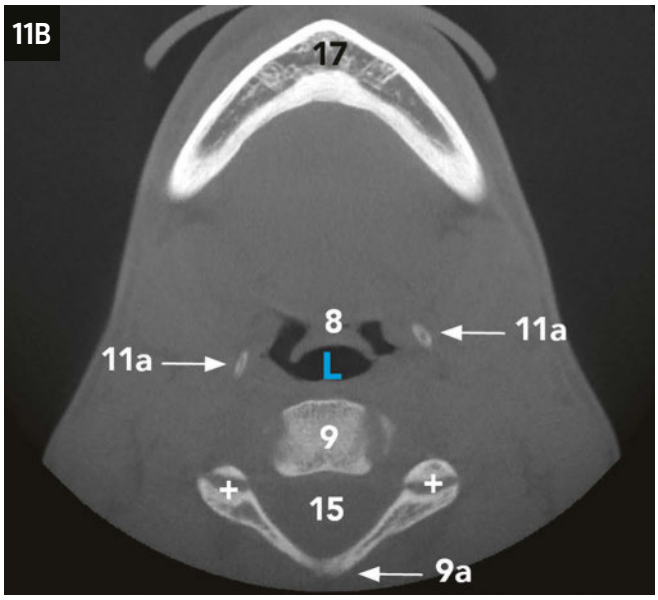
11B
17
8
11a
11a
L
9
+
+
15
9a

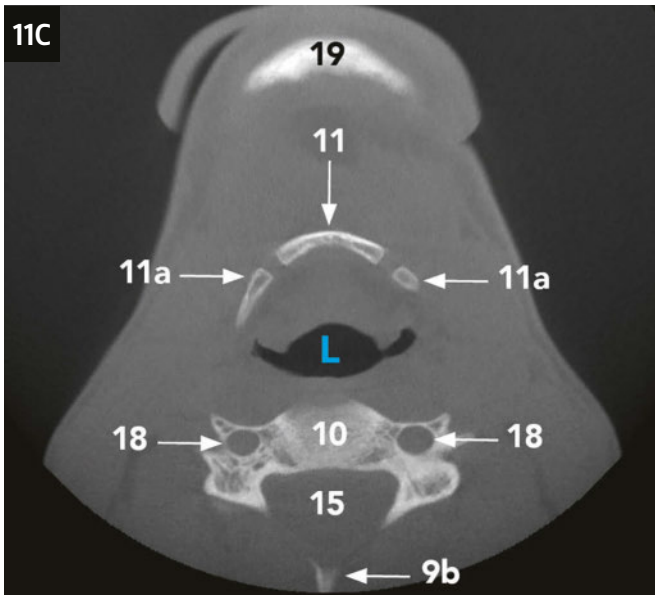
11C
19
11
11a
11a
L
18
10
18
15
9b

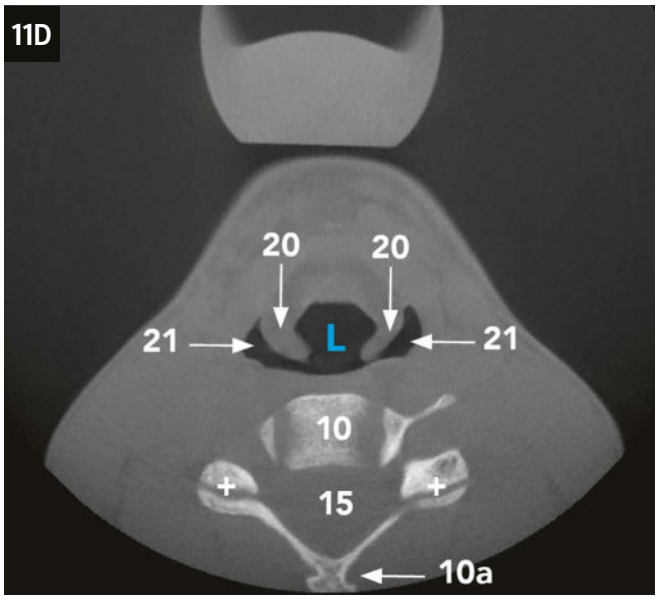
11D
20
20
21
L
21
10
+
15
+
10a

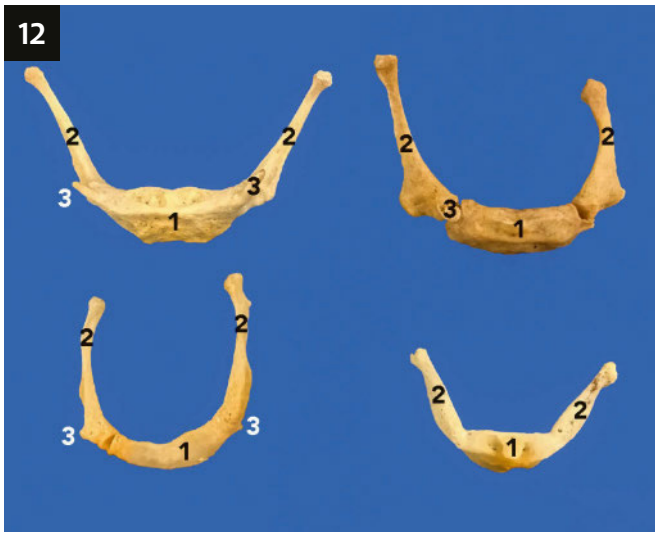

Fig. 12 Variations of hyoid bones (image courtesy of Dr. Bob Mann, Department of Anatomy, University of Hawaii John A. Burns School of Medicine, Honolulu, USA).
1 = median body; 2 = greater horn; 3 = lesser horn.

Fig. 13 Hyoid bone of a 47-year-old female: (A) 3D rendering image showing position of hyoid bone (dotted circle); (B) axial CBCT image at the level of the chin–C3 axis; (C) reformatted CBCT image along the left body of the hyoid bone. L = laryngopharynx.
1 = chin; 2 = median body of hyoid bone; 3 = greater horn of hyoid bone; 4 = epiglottis; 5 = vallecula epiglottica; 6 = body of C3; 7 = lesser horn of hyoid bone; 8 = soft palate; 9 = dorsum of tongue; 10 = base of tongue.

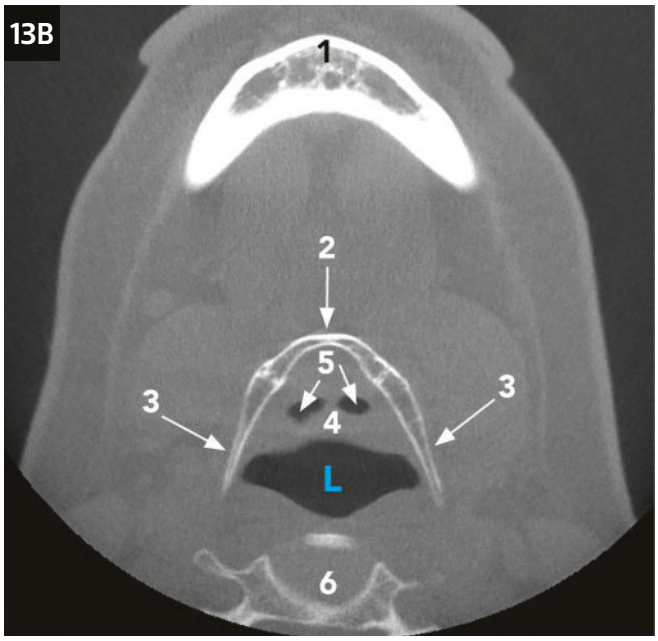

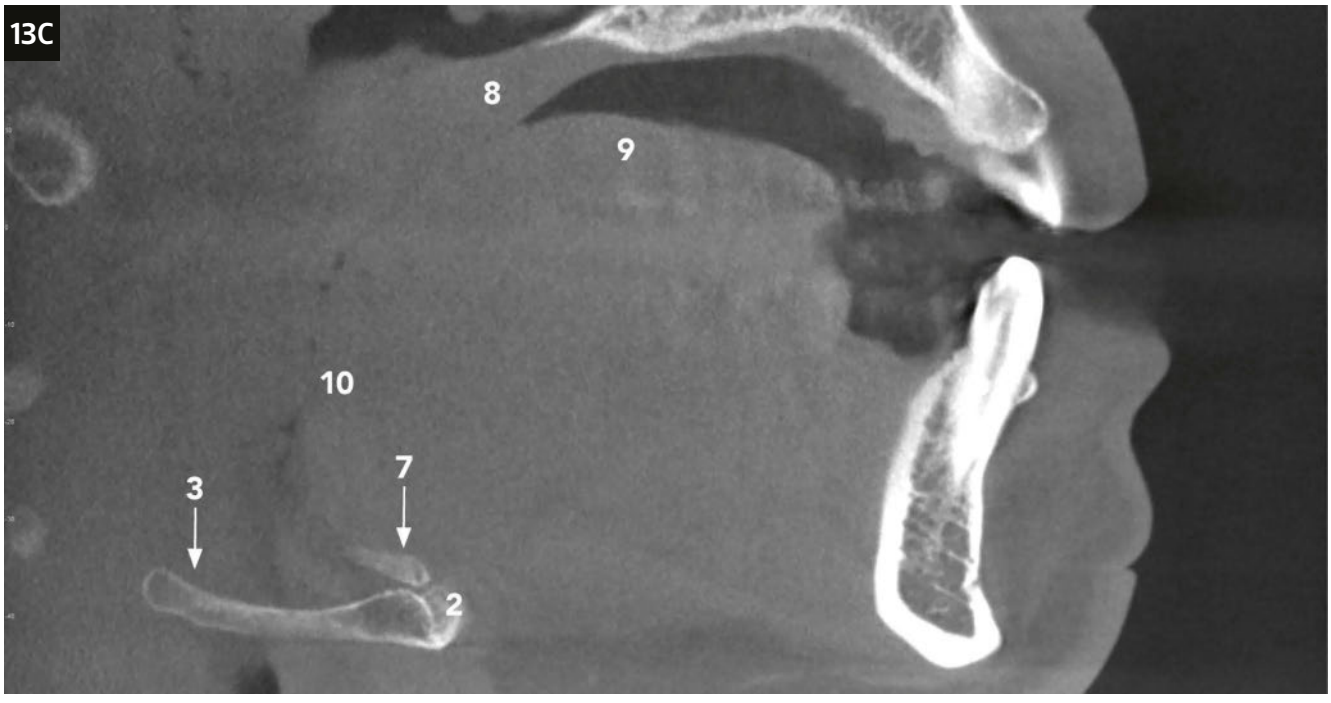

pophysial joints), and a posterior arch. In addition, and in contrast to thoracic and lumbar vertebrae, C3–C6 are characterized by a split posterior process – i.e., bifid spinous process – and the presence of a transverse foramen on each side lateral to the vertebra body. Zibis et al. (2016) reported unexpectedly high rates of hypoplastic, double or triple transverse foramina in cervical vertebrae. The zygapophysial joints are formed by the inferior articular process of the vertebra above and the superior articular process of the vertebra below. Fibroadipose menisciods intervene between the articular cartilages of these joints. The zygapophysial joints are planar, and at typical cervical levels are oriented at about 40° to the coronal and transverse planes, so that they face backwards and upwards (Bogduk & Mercer 2000).

C7

This vertebra is the lowest but strongest of the seven cervical vertebrae *(vertebra prominens)*. It has the largest body and also presents a marked, single and non-bifid posterior spinous process that can be easily palpated through the skin. Although C7 is closest to the thoracic vertebrae in terms of anatomical position and configuration, it also contains a bilateral transverse foramen, which is absent in the thoracic vertebrae. However, unlike the rest of the cervical vertebrae, the vertebral artery does not traverse this transverse foramen (Waxenbaum & Futterman 2018).

Hyoid bone

The hyoid bone is commonly seen in CBCT images of the lower face or mandible/neck region (Fig. 12 and 13). The hyoid bone is the only bone of the head neck region that does not articulate with other bones. It is connected to the pharynx, mandible, and skull by muscles and ligaments. Tension generated in these structures due to movement of the head and body and resulting from oral and tongue function will change its position (da Costa et al. 2017). The gross anatomy of the hyoid bone consists of a median body, two ventrally located minor horns, and two dorsally located major horns (Soerdjbalie-Maikoe & van Rijn 2008).

The hyoid bone is located above the larynx at the height of the third (C3) or fourth cervical vertebra (C4) (Ito et al. 2012; Mirjalili et al. 2012; Liu et al. 2017). The hyoid bone supports the base of the tongue and is involved in breathing, chewing, and swallowing as well as in the muscle movements associated with articulation. Accordingly, it plays an important role for humans (Ito et al. 2012).

The shape of the hyoid bone is characterized by a horseshoe or U-shape (Ito et al. 2012) composed of a rectangular body anteriorly from which bilateral small (lesser horns, *cornua minoria*) and large bone projections (greater horns, *cornua majoria*) extend posteriorly. The hyoid bone is connected to the nearby structures by ligaments and muscles, without any synovial joints, thus seemingly floating in the neck region (Radunovic et al. 2018).

Morphometrics of the hyoid bone were assessed in 88 intact hyoid bones taken from cadavers and in 92 hyoid bones with CT scan images (Fakhry et al. 2013). Dimensions were significantly greater in men than in women; i.e., length 3.9 vs. 3.3 cm, and width 4.2 vs. 3.9 cm. In contrast, the angle between the greater horns was larger in females (44.1°) compared to males (38.8°). The length of the hyoid bone was positively correlated with the height and weight of subjects.

Fig. 14 Skull presenting bilateral elongated styloid processes (image courtesy of Dr. Bob Mann, Department of Anatomy, University of Hawaii John A. Burns School of Medicine, Honolulu, USA).

Muscles attaching to the hyoid bone are divided into supra- and infrahyoid muscles. Suprahyoid muscles include the geniohyoid, mylohyoid, stylohyoid, hyoglossus and digastric. The tendon between the anterior and posterior bellies of the digastric muscle passes through a fascial sling that is connected to the greater horn of the hyoid bone. Infrahyoid muscles comprise the omohyoid, sternohyoid and thyrohyoid.

Frequently, a bony projection (also termed *lingula*) is found in the center of the upper surface of the hyoid body. The site of incidence is the same where the thyrolingual duct reaches the hyoid bone, and this process is considered a residue of the thyrolingual duct (Ito et al. 2012).

Styloid process

Although not a direct component of the pharyngocervical region, the styloid process is regularly visible on CBCT images depicting that region. The bilateral styloid process impresses as a needle-like bony projection originating from the bottom of the petrous temporal bone just anteromedial to the stylomastoid foramen and lateral to the jugular foramen, respectively (von Arx & Lozanoff 2017) (Fig. 14). Occasionally, the styloid process is partially (proximal part) or totally absent (Basekim et al. 2005; Onbas et al. 2005). The styloid process serves as attachment of the stylohyoid as well as of the stylomandibular ligament and of three muscles, i.e., stylohyoid, styloglossus, and stylopharyngeus. These structures affect and facilitate movements of the tongue, pharynx, hyoid bone, and mandible (Abuhaimed & Menezes 2019).

On axial slices, the styloid process might be confused with calcifications in the upper lateral neck area or with the hyoid bone. However, observing the symmetrical appearance, the distance between left and right styloid processes is usually 6–8 cm, whereas the side-to-side space of the hyoid bone is in the range of 3 to 4 cm.

Multiple anatomical and radiographic studies have evaluated the morphology and dimensions of the styloid processes

Tab. I Summary of studies evaluating the dimensions of the styloid process (StP)

Authors/year	Material	Method	Mean length of StP (mm)	Mean angle of StP (°)	Comments
Basekim et al. 2005	138 patients with CT	Measurements were taken on 3D reconstructed images; angle assessed in coronal plane	28.3 ± 7.6 (15.8–54.8) Males: 29.1 ± 7.9 Females: 26.8 ± 6.6	69.5 ± 4.3 (60.6–84.1) Males: 70.5 ± 4.2 Females: 68.7 ± 4.2	StP were absent unilaterally in three cases and bilaterally in one case Lengths and angles did not differ significantly with regard to gender
Onbas et al. 2005	283 patients with multidetector CT	Measurements were taken on 3D reconstructed images; angles assessed in coronal and sagittal planes	26.8 ± 10.0 (0–62)	Angle in coronal plane: 72.7 ± 6.6 (55–90.5) Angle in sagittal plane: 93.5 ± 6.9 (76–110)	In 7 individuals, the StP was entirely absent on one side; in 9 individuals, the StP was duplicated (4 uni- and 5 bilateral)
Balcioglu et al. 2009	Bilateral StP in 22 formalin-fixed cadavers; and dry skulls with 41 measurable StP	Digital caliper for length measurement	22.5 ± 4.24	–	StP was considered elongated (> 30 mm) in 3.3%
Krmpotic Nemanic et al. 2009	88 macerated skulls	NA	Right side: 11–20y: 2.3 ± NA 21–60y: 14.2 ± 10.5 62–85y: 16.3 ± 10.0 Left side: 11–20y: 2.5 ± NA 21–60y: 13.9 ± 10.5 62–85y: 17.3 ± 11.3	–	Statistically significant positive association between StP length and age
Cullu et al. 2013	160 patients with multidetector CT	NA	Overall: 28.4 ± 5.5 Males: 29.2 ± 5.6 Females: 27.2 ± 5.2	–	Individual length varied from 18 to 57 mm; gender difference was statistically significant
Ekici et al. 2013	805 patients with multidetector CT	Measurements were taken on 3D reconstructed images; angles assessed in coronal and sagittal planes	All: 31.2 ± 11.9 (0–74) Males: 33.2 ± 13.2 Females: 29.6 ± 10.5	Angle in coronal plane: 70.5 ± 4.2 (57–82.5) Angle in sagittal plane: 87.6 ± 6.5 (68–115)	StP was considered elongated (> 30 mm) in 56%; in 10 cases (1.3 %), a bony StP was entirely absent (7 unilateral and 3 bilateral); gender difference was statistically significant
Öztunc et al. 2014	208 patients with CBCT	Radiological measurements of length and angle (in coronal plane between base of both StP and axis of StP)	Males: 29.0 ± 9.5 Females: 30.0 ± 10.9	Elongated cases: 68 ± 3.76 Non-elongated cases: 70 ± 4.12	StP was considered elongated (> 30 mm) in 54%; gender difference was not statistically significant
Patil et al. 2014	114 dry skulls	Digital Vernier caliper for measurement of length and distances between bases and tips of StP; angles were determined on digital images	25.8 ± 7.8	Angle in sagittal plane: 62.5 ± 8.5 Angle in axial plane: 74.2 ± 6.5	Distance bases: 68.0 ± 5.6 mm Distance tips: 46.5 ± 7.4 mm
Vadgaonkar et al. 2015	110 dry skulls	Digital Vernier caliper for measurement of length and distances between bases and tips of StP	Right side: 17.8 ± 9.3 Left side: 18.2 ± 5.6	–	Distance bases: 68.9 ± 4.3 mm Distance tips: 60.7 ± 2.4 mm In 4.5%, StP was considered elongated (> 30 mm); Longest StP was 50.0 mm

Tab. I Summary of studies evaluating the dimensions of the styloid process (StP) continued

Authors/year	Material	Method	Mean length of StP (mm)	Mean angle of StP (°)	Comments
Yilmaz et al. 2015	100 patients with multidetector CT	Measurements were taken on 3D volume-rendered images	Right side: 23.0 ± 8.6 Left side: 23.1 ± 7.8	Angle in coronal plane Right side: 71.7 ± 6.2 Left side: 71.2 ± 6.9	Distance bases: 81.4 ± 5.7 mm
Buyuk et al. 2018	1000 patients with CBCT	Length and angles were measured on multiplanar reconstructions using software tools	Males: 36.4 ± 10.0 Females: 32.8 ± 8.8	Angle in coronal plane Males: 72.2 ± 6.4 Females: 70.3 ± 6.6 Angle in sagittal plane Males: 74.0 ± 8.0 Females: 70.4 ± 8.1	All gender differences were statistically significant
Zokaris et al. 2019	805 digital panoramic radiographs	Computer software for measuring length	Males: 28.4 ± 8.5 Females: 26.0 ± 7.7	–	All patients were 17- to 21-years-old; StP was considered elongated (> 30 mm) in 30.6%; gender difference was not statistically significant

(Balcioglu et al. 2009; Krmpotic Nemanic et al. 2009; Cullu et al. 2013; Öztunc et al. 2014; Patil et al. 2014; Vadgaonkar et al. 2015; Yilmaz et al. 2015; Zokaris et al. 2019) (Tab. I). Most authors consider a styloid process longer than 30 mm as an elongated process whereas Eagle, after whom the Eagle's syndrome is named, used a threshold value of 25 mm (Eagle 1948; Cullu et al. 2013). In contrast, the stylohyoid syndrome usually describes the partial or complete ossification of the stylohyoid ligament. Others have coined the term stylohyoid complex (SHC), including the styloid process, the ossified stylohyoid ligament, as well as the lesser horn of the hyoid bone (Ledesma-Montes et al. 2018). As such, the SHC is an anatomic structure rich in variations including various lengths of the styloid process (absence, duplicated or elongated), various degrees of ossification of the stylohyoid ligament, and various fusions of the SHC portions (Ekici et al. 2013; Bornstein et al. 2019).

Discussion

CBCT imaging has become a frequent method for diagnosis, treatment planning, and follow-up assessment in dentistry. This radiographic method inevitably exhibits anatomical structures outside the region of interest – i.e., extraoral anatomy in CBCT. This last part of a 4-part literature review addresses the pharyngocervical region.

The pharynx includes the upper portions of the digestive and respiratory tracts. Dentists must be familiar with the normal anatomy of the airway so that any incidental abnormalities can be recognized. A systematic evaluation of the various compartments of the upper airway is important to recognize anatomic and pathologic alterations (White et al. 2015). Indeed, incidental airway abnormalities are detected on CBCT scans in 21–52% of patients, underscoring the need for a careful analysis of the airway on these imaging exams (White et al. 2015).

Automatic edge detection of the pharynx based on CBCT imaging has facilitated advances in quantification of airway size and shape (Celenk et al. 2010). A recent systematic review demonstrated that 3D analysis of the upper airway using CBCT is accurate and reliable (Guijarro & Swennen 2011). However, it was found that the anatomical definitions of the airway subregions from the nasal and oral cavities to the larynx were variable among different authors. Discrepancies mostly arise when the pharyngeal subregions are either differentiated by natural anatomical borders versus easily identifiable radiographic landmarks (Guijarro & Swennen 2013). For example, some authors define the lower border of the nasopharynx as the plane through the posterior nasal spine parallel to the Frankfort plane, whereas others denote the soft palate or the tip of the uvula as the lower nasopharyngeal boundary.

Another critical issue is patient positioning during CT and CBCT acquisition since this has an effect on the location of anatomical structures like the hyoid bone and may significantly change the dimensions of the posterior airway space (Ayoub et al. 2019). Similarly, if the patient were to swallow during the scan acquisition, the soft palate would appear higher and juxtaposed against the posterior pharyngeal wall, thereby reducing the velopharyngeal airspace. Thus, interpretation of the airway dimensions must consider such modifying factors (White et al. 2015). Furthermore, the patient's position in which the CT/CBCT scan is acquired – i.e., supine versus standing/sitting – may also impact the airway morphology. The gravitational forces on the tongue as well as on the soft palate are expected to be different in a supine position compared to a standing position. Consequently, airway morphology imaged with the patient in the supine position is more relevant of the airway morphology during sleep (White et al. 2015).

Changes in the positioning of the mandible (physiological, surgical, or due to orthodontic treatment) are also accompanied by changes in the positioning of the hyoid bone. This mechanism of compensation of hyoid position may result in changes in the dimension of the pharyngeal airway and may therefore have clinical implications (da Costa et al. 2017). In the context of obstructive sleep apnea syndrome (OSAS), numerous reports address the pharyngeal airway space. Risk factors

for the disease are conditions that reduce the size of the resting pharynx or increase airway collapsibility (Veasey & Rosen 2019). The reader is directed to the pertinent literature.

Acknowledgement

The authors thank Bernadette Rawyler, medical illustrator, and Ines Badertscher, media designer, School of Dental Medicine, University of Bern, Bern, Switzerland, for the illustrations and preparation of figures. The authors acknowledge the generous donation of the anatomical materials by anonymous individuals in the Willed Body Program, the University of Hawaii John A. Burns School of Medicine, Honolulu, USA. We also thank the following people from the Department of Anatomy, University of Hawaii John A. Burns School of Medicine, Honolulu, USA: Jesse Thompson and Beth Lozanoff for the 3D models (see web links), and Bob Mann and Beth Lozanoff for providing Figures 12 and 14.

The authors also acknowledge Dr. Odette Engel Brügger, Oral Surgeon in Nidau, Switzerland, for the French translation of the summary.

Conflict of interest

The authors declare that there are no conflicts of interest related to this review.

Zusammenfassung

In dieser vierten und letzten Arbeit über die extraorale Anatomie in der Digitalen Volumentomographie (DVT) wird die pharyngozervikale Region diskutiert. Dieses anatomische Gebiet umfasst die oberen Atemwege, den Pharynx sowie die Halswirbelsäule. Bei grösseren Volumina können diese Strukturen auf DVT-Bildern der Kieferregionen abgebildet werden.

Der Pharynx (Rachen, Schlund) reicht von der Schädelbasis bis zum Eingang der Speiseröhre. Die Länge beträgt ca. 13 cm und die Breite 4 cm. Strukturell ist der Pharynx eine muskulofasziale Röhre, hauptsächlich bestehend aus den drei Konstriktorenmuskeln und deren Faszien *(Musculus constrictor pharyngis superior, medius et inferior).* Anatomisch wird der Rachen in drei Abschnitte eingeteilt: Nasopharynx, Oropharynx und Laryngopharynx.

Der Nasopharynx kommuniziert als oberster Teil des Rachens über die Choanen mit den beiden Nasenhöhlen. Die Spitze der Uvula entspricht der untersten Begrenzung des Nasopharynx. Die Rachenmandeln (Adenoid, *Tonsilla pharyngea*) liegen ganz oben in der hinteren Wand des Nasopharynx. In den Seitenwänden finden sich bilateral die Öffnungen der *Tuba auditiva* (Eustachische Röhre) als Verbindung zum Mittelohr. Der freie Rand des Tubenknorpels imponiert als halbkreisförmige Erhebung. Posterior davon findet sich eine Einziehung, *Recessus pharyngeus,* auch als Rosenmüller-Grube bezeichnet.

Der Oropharynx entspricht dem mittleren Abschnitt des Rachens und kommuniziert über den *Isthmus faucium* mit der Mundhöhle. Unten reicht der Oropharynx bis zum Kehldeckel (Epiglottis). Der Zungengrund sowie die Gaumenmandeln *(Tonsillae palatinae),* die zwischen dem *Musculus palatoglossus* und dem *Musculus palatopharyngeus* liegen, gehören ebenfalls zum Oropharynx.

Der Laryngopharynx ist der unterste Teil des Rachens und liegt hinter dem Kehlkopf (Larynx). Die Epiglottis bildet die obere Begrenzung (Höhe ca. C3/C4) und der Oesophagus-Eingang die untere Begrenzung (Höhe ca. C5/C6) des Laryngopharynx. Zwischen den unteren Epiglottisseitenrändern *(Plicae aryepiglotticae)* und den lateralen Wänden des Laryngopharynx findet sich beidseits eine tiefe Einziehung, der sogenannte *Recessus* oder *Sinus piriformis.*

Die Halswirbelsäule umfasst die sieben Halswirbel C1 bis C7. Die zwei obersten Halswirbel, Atlas (C1) und Axis (C2), haben eine spezielle Morphologie, während die restlichen Halswirbel eine ähnliche Form wie die Brustwirbel aufweisen. Der unterste Halswirbel (C7) hat den grössten Wirbelkörper und einen prominenten Fortsatz nach posterior *(Processus spinosus),* der gut durch die Haut tastbar ist. Die Halswirbel werden oft als Referenzen für die Lagebestimmung von Rachenstrukturen verwendet. Dabei ist zu beachten, dass die Körperlage (liegend versus sitzend) bzw. die Kopfposition (Flexion versus Extension) diese Referenzhöhen beeinflussen können.

Das Zungenbein *(Os hyoideum)* kommt regelmässig zur Darstellung auf DVT-Bildern des Unterkiefers bzw. des Halsbereichs. Über mehrere Muskeln und Ligamente ist das Hyoid mit Unterkiefer, Pharynx und Schädel verbunden. Das Zungenbein besteht aus einem zentralen Körper sowie jeweils zwei kleinen und zwei grossen Fortsätzen und liegt etwa auf Höhe C3/C4. In der Form gleicht das Zungenbein einem Hufeisen und weist durchschnittlich eine Länge und Breite von 4 cm auf.

Der *Processus styloideus* ist ein länglicher, nadelförmiger Knochenfortsatz, der von der Unterfläche des *Os temporale* in anteroinferiorer Richtung zum Halsbereich zieht. Diese Struktur wird regelmässig auf DVT-Bildern der pharyngozervikalen Region dargestellt. Auf den axialen Schnittbildern kann es zu Verwechslungen mit Kalzifikationen im oberen lateralen Halsbereich kommen. Der *Processus styloideus* dient als Ansatz für diverse Muskeln und Ligamente. Letztere können teilweise oder vollständig verknöchern (Stylohyoid-Syndrom), oder der *Processus styloideus* weist eine überdurchschnittliche Länge auf (Eagle-Syndrom).

Résumé

Ce quatrième et dernier travail au sujet de l'anatomie extraorale au CBCT présente la zone pharyngo-cervicale. Cette région inclut les voies respiratoires supérieures, le pharynx et la colonne cervicale – ces structures pouvant être représentées dans les grands volumes de CBCT de la région maxillaire.

Le pharynx (gorge) s'étend de la base du crâne à l'entrée de l'œsophage. Sa longueur est d'environ 13 cm et sa largeur de 4 cm. Le pharynx est un conduit musculo-membraneux et se compose des trois muscles constricteurs et de leurs fascias *(Musculus constrictor pharyngis superior, medius,* et *inferior).* Anatomiquement, le pharynx est subdivisé en trois parties : le nasopharynx, l'oropharynx, et le laryngopharynx.

Le nasopharynx, la partie supérieure du pharynx, communique vers l'avant avec les deux fosses nasales via les choanes. La pointe de l'uvule représente sa limite inférieure. Les amygdales pharyngiennes (adénoïdes, *Tonsilla pharyngea*) se trouvent dans la partie supérieure de la paroi postérieure du pharynx. Les orifices de la trompe d'Eustache *(Tuba auditiva)* – communication avec l'oreille moyenne – sont situés de chaque côté sur les parois latérales du nasopharynx. Le bord libre du cartilage de la trompe forme une élévation semi-circulaire sur cette paroi. En arrière de celle-ci se trouve le récessus pharyngien, la fossette de Rosenmüller.

L'oropharynx correspond à la partie moyenne du pharynx et communique avec la bouche par l'*Isthmus faucium.* Il s'étend vers le bas jusqu'à l'épiglotte. La base de la langue et les amygdales palatines, qui se trouvent entre les *Musculus palatoglossus*

et *Musculus palatopharyngeus,* appartiennent aussi à l'oropharynx.

Le laryngopharynx est la partie inférieure de la gorge et se trouve à l'arrière du larynx. Il s'étend de l'épiglotte (environ à hauteur C3/C4) jusqu'à l'orifice de l'œsophage (environ à hauteur C5/C6). On trouve un fort récessus entre les bords inférieurs latéraux de l'épiglotte et les parois latérales du laryngopharynx, le *Sinus piriformis.*

La colonne cervicale se compose des sept vertèbres cervicales (C1–C7). Les deux premières vertèbres cervicales, l'atlas (C1) et l'axis (C2), ont une morphologie particulière, tandis que les autres vertèbres cervicales ont une forme similaire aux vertèbres thoraciques. La vertèbre cervicale inférieure (C7) est caractérisée par un corps vertébral plus grand et un processus épineux très long *(Processus spinosus),* qui est aisément palpable sous la peau. Les vertèbres cervicales sont souvent utilisées comme point de référence pour l'orientation des structures pharyngiennes. Veuillez noter que la position du corps (couchée ou assise) et la position de la tête (flexion ou extension) peuvent influencer ces points de référence.

L'os hyoïde est régulièrement visible sur les images cone beam de la mandibule et du cou. Plusieurs muscles et ligaments relient l'os hyoïde à la mandibule, au pharynx et au crâne. L'os hyoïde se compose d'un corps central et de deux grandes et deux petites cornes. Il est situé au niveau de C3 ou C4, présente la forme d'un fer à cheval et a une longueur et largeur d'environ 4 cm.

L'apophyse styloïde est une protubérance osseuse allongée et pointue sur la face inférieure de l'os temporal. Elle se prolonge en direction antéro-inférieure vers le cou. Cette structure anatomique est régulièrement visible sur les images cone beam de la zone pharyngo-cervicale. On peut la confondre avec des calcifications dans les parties supérieures et latérales du cou dans les coupes horizontales. Le rôle principal de l'apophyse styloïde est l'insertion de plusieurs muscles et ligaments. Ces derniers peuvent présenter une ossification partielle ou complète (syndrome du processus styloïde). L'apophyse styloïde peut aussi avoir une longueur supérieure à la moyenne (syndrome d'Eagle).

References

Abuhaimed A K, Menezes R G: Anatomy, Head and Neck, Styloid Process. StatPearls Publishing, Treasure Island (FL) (2019)

Ayoub N, Eble P, Kniha K, Peters F, Möhlenrich S C, Goloborodko E, Hölzle F, Modabber A: Three-dimensional evaluation of the posterior airway space: differences in computed tomography and cone beam computed tomography. Clin Oral Invest 23: 603–609 (2019)

Balcioglu H A, Kilic C, Akyol M, Ozan H, Kokten G: Length of the styloid process and anatomical implications for Eagle's syndrome. Folia Morphol (Warsz) 68: 265–270 (2009)

Basekim C C, Mutlu H, Güngör A, Silit E, Pekkafali Z, Kutlay M, Colak A, Oztürk E, Kizilkaya E: Evaluation of styloid process by three-dimensional computed tomography. Eur Radiol 15: 134–139 (2005)

Becker A M, Hwang P H: Endoscopic endonasal anatomy of the nasopharynx in a cadaver model. Int Forum Allergy Rhinol 3: 319–324 (2013)

Bogduk N: Functional anatomy of the spine. Handb Clin Neurol 136: 675–688 (2016)

Bogduk N, Mercer S R: Biomechanics of the cervical spine. I: Normal kinematics. Clin Biomech 15: 633–648 (2000)

Bornstein M M, Yeung Awk, Tanaka R, Curtin J P: Calcified stylohyoid-complex – clinical and radiographic findings (in German). Swiss Dent J 129: 726–727 (2019)

Buyuk C, Gunduz K, Avsever H: Morphological assessment of the stylohyoid complex variations with CBCT in a Turkish population. Folia Morphol (Warsz) 77: 79–89 (2018)

Celenk M, Farrell M L, Eren H, Kumar K, Singh G D, Lozanoff S: Upper airway detection and visualization from cone beam image slices. J Xray Sci Technol 18: 121–135 (2010)

Civelek E, Kiris T, Hepgul K, Canbolat A, Ersoy G, Cansever T: Anterolateral approach to the cervical spine: major anatomical structures and landmarks. Technical note. J Neurosurg Spine 7: 669–678 (2007)

Cullu N, Deveer M, Sahan M, Tetiker H, Yilmaz M: Radiological evaluation of the styloid process length in the normal population. Folia Morphol (Warsz) 72: 318–321 (2013)

da Costa E D, Roque-Torres G D, Brasil D M, Boscolo F N, de Almeida S M, Ambrosano G M: Correlation between the position of hyoid bone and subregions of the pharyngeal airway space in lateral cephalometry and cone beam computed tomography. Angle Orthod 87: 688–695 (2017)

Eagle W W: Elongated styloid process; further observations and a new syndrome. Arch Otolaryngol 47: 630–640 (1948)

Ekici F, Tekbas G, Hamidi C, Onder H, Goya C, Cetincakmak M G, Gumus H, Uyar A, Bilici A: The distribution of stylohyoid chain anatomic variations by age groups and gender: an analysis using MDCT. Eur Arch Otorhinolaryngol 270: 1715–1720 (2013)

Fakhry N, Puymerail L, Michel J, Santini L, Lebreton-Chakour C, Robert D, Giovanni A, Adalian P, Dessi P: Analysis of hyoid bone using 3D geometric morphometrics: An anatomical study and discussion of potential clinical implications. Dysphagia 28: 435–445 (2013)

Fossum C C, Chintakuntlawar A V, Price D L, Garcia J J: Characterization of the oropharynx: Anatomy, histology, immunology, squamous cell carcinoma and surgical resection. Histopathology 70: 1021–1029 (2017)

Guijarro-Martinez R, Swennen G R: Cone-beam computerized tomography imaging and analysis of the upper airway: A systematic review of the literature. Int J Oral Maxillofac Surg 40: 1227–1237 (2011)

Guijarro-Martinez R, Swennen G R: Three-dimensional cone beam computed tomography definition of the anatomical subregions of the upper airway: A validation study. Int J Oral Maxillofac Surg 42: 1140–1149 (2013)

Gun R, Ozer E: Surgical anatomy of oropharynx and supraglottic larynx for transoral robotic surgery. J Surg Oncol 112: 690–696 (2015)

Inamoto Y, Saitoh E, Okada S, Kagaya H, Shibata S, Baba M, Onogi K, Hashimoto S, Katada K, Watanapan P, Palmer J B: Anatomy of the larynx and pharynx: Effects of age, gender and height revealed by multidetector computed tomography. J Oral Rehabil 42: 670–677 (2015)

Ito K, Ando S, Akiba N, Watanabe Y, Okuyama Y, Moriguchi H, Yoshikawa K, Takahashi T, Shimada M: Morphological study of the human hyoid bone with three-dimensional CT images – Gender difference and age-related changes. Okajimas Folia Anat Jpn 89: 83–92 (2012)

Kaiser J T, Lugo-Pico J G: Anatomy, Head and Neck, Cervical vertebrae. StatPearls Publishing, Treasure Island (FL) (2019)

Krmpotic Nemanic J, Vinter I, Ehrenfreund T, Marusic A: Postnatal changes in the styloid process, vagina processus styloidei, and stylomastoid foramen in relation to the function of muscles originating from the styloid process. Surg Radiol Anat 31: 343–348 (2009)

Ledesma-Montes C, Hernandez-Guerrero J C, Jimenez-Farfan M D: Length of the ossified stylohyoid complex and Eagle syndrome. Eur Arch Otorhinolaryngol 275: 2095–2100 (2018)

Liu J M, Du L X, Xiong X, Chen X Y, Zhou Y, Long X H, Huang S H, Liu Z L: Radiographic evaluation of the reliability of neck anatomic structures as anterior cervical surgical landmarks. World Neurosurg 103: 133–137 (2017)

Lomoschitz F, Schima W, Schober E, Pokieser P, Youssefzadeh S, Kainberger F, Czerny C, Imhof H: The Pharynx. The imaging of its normal anatomy (article in German). Radiologe 40: 601–609 (2000)

Lun H M, Zhu S Y, Liu R C, Gong J G, Liu Y L: Investigation of the upper airway anatomy with ultrasound. Ultrasound Q 32: 86–92 (2016)

Mirjalili S A, McFadden S L, Buckenham T, Stringer M D: Vertebral levels of key landmarks in the neck. Clin Anat 25: 851–857 (2012)

Nemec S F, Krestan C R, Noebauer-Huhmann I M, Formanek M, Frühwald J, Peloschek P, Kainberger F, Czerny C: Radiological normal anatomy of the larynx and pharynx and imaging techniques (article in German). Radiologe 49: 8–16 (2009)

Ogawa T, Enciso R, Shintaku W H, Clark G T: Evaluation of cross-section airway configuration of obstructive sleep apnea. Oral Surg Oral Med Oral Pathol Oral Radiol Endod 103: 102–108 (2007)

Onbas O, Kantarci M, Murat Karasen R, Durur I, Cinar Basekim C, Alper F, Okur A: Angulation, length, and morphology of the styloid process of the temporal bone analyzed by multidetector computed tomography. Acta Radiol 46: 881–886 (2005)

Öztunc H, Evlice B, Tatli U, Evlice A: Cone-beam computed tomographic evaluation of styloid process: a retrospective study of 208 patients with orofacial pain. Head Face Med 10: 5 (2014)

Patil S, Ghosh S, Vasudeva N: Morphometric study of the styloid process of temporal bone. J Clin Diagn Res 8: AC04–6 (2014)

Radunovic M, Vukcevic B, Radojevic N: Asymmetry of the greater cornua of the hyoid bone and the superior thyroid cornua: A case report. Surg Radiol Anat 40: 959–961 (2018)

Raol N, Hartnick C J: Anatomy and physiology of velopharyngeal closure and insufficiency. Adv Otorhinolaryngol 76: 1–6 (2015)

Shigeta Y, Ogawa T, Tomoko I, Clark G T, Enciso R: Soft palate length and upper airway relationship in OSA and non-OSA subjects. Sleep Breath 14: 353–358 (2010)

Soerdjbalie-Maikoe V, van Rijn R R: Embryology, normal anatomy, and imaging techniques of the hyoid and larynx with respect to forensic purposes: A review article. Forensic Sci Med Pathol 4: 132–139 (2008)

Vadgaonkar R, Murlimanju B V, Prabhu L V, Rai R, Pai M M, Tonse M, Jiji P J: Morphological study of styloid process of the temporal bone and its clinical implications. Anat Cell Biol 48: 195–200 (2015)

Veasey S C, Rosen I M: Obstructive sleep apnea syndrome in adults. N Engl J Med 380: 1442–1449 (2019)

von Arx T, Lozanoff S: Clinical Oral Anatomy – A Comprehensive Review for Dental Practitioners and Researchers. 1st edition, Springer International, Switzerland (2017)

Waxenbaum J A, Futterman B: Anatomy, Back, Cervical Vertebrae. StatPearls Publishing, Treasure Island (FL) (2019)

White S M, Huang C J, Huang S C, Sun Z, Eldredge J D, Mallya S M: Evaluation of the upper airway morphology: The role of cone beam computed tomography. J Calif Dent Assoc 43: 531–539 (2015)

Wysocki J, Bubrowski M, Reymond J, Kwiatkowski J: Anatomical variants of the cervical vertebrae and the first thoracic vertebra in man. Folia Morphol (Warsz) 62: 357–363 (2003)

Yilmaz M T, Akin D, Cicekcibasi A E, Kabakci A D, Seker M, Sakarya M E: Morphometric analysis of styloid process using multidetector computed tomography. J Craniofac Surg 26: e438–443 (2015)

Zibis A H, Mitrousias V, Baxevanidou K, Hantes M, Karachalios T, Arvanitis D: Anatomical variations of the foramen transversarium in cervical vertebrae: Findings, review of the literature, and clinical significance during cervical spine surgery. Eur Spine J 25: 4132–4139 (2016)

Zokaris N, Siska I, Natsis K, Piagkou M, Lazaridis N, Skolka A, Piehslinger E: Investigation of the styloid process length in a Greek population. Folia Morphol (Warsz) 78: 378–388 (2019)